Semi-transparent wide band gap $Cu_2ZnGe(S,Se)_4$ thin-film solar cells: Role of the sulfurization process

*Andrea Ruiz-Perona[1, +], David Palma-Lafuente[1], Yudania Sánchez[2], Maxim Guc[2], Tim Kodalle[3, x], Mohamed Ould Salem[2], Marcel Placidi[2,4], Rosalia Serna[5], Alejandro Pérez-Rodríguez[2,6], José Manuel Merino[1], Raquel Caballero[1,5]**

[1]Universidad Autónoma de Madrid, Departamento de Física Aplicada, C/ Francisco Tomás y Valiente 7, 28049 Madrid, Spain

[2]IREC, Catalonia Institute for Energy Research, C/ Jardins de les Dones de Negre 1, 08930 Barcelona, Spain

[3]PVcomB-Helmholtz Zentrum Berlin für Materialien und Energie, Schwarzschildstrasse 3, 12489 Berlin, Germany

[4]Universitat Politècnica de Catalunya, Departament d'Enginyeria Electrònica & Barcelona Center for Multiscale Science & Engineering, Av Eduard Maristany 10-14, 08019 Barcelona, Spain

[5]Instituto de Óptica "Daza de Valdés"-CSIC, C/ Serrano 121, 28006 Madrid, Spain

[6]Universitat de Barcelona, IN2UB, Department d`Enginyeria Electrònica y Biomèdica, C/ Martí i Franquès 1-11, 08028 Barcelona, Spain

[+]Current address: Andrea Ruiz Perona, National Institute of Material Science (NIMS), Namiki 1-choume, Tsukuba, Ibaraki Japan

[x]Current address: Tim Kodalle, Molecular Foundry, Lawrence Berkeley National Laboratory, 1 Cyclotron Road, Berkeley, CA-94608, USA.

*E-mail: raquel.caballero@csic.es

Conflict of Interest. The authors declare no conflict of interest.

Data Availability Statement. The data that support the results of this study are available from the corresponding author upon reasonable request.

Keywords: copper zinc germanium sulfoselenides, wide band gap energies, semitransparent solar cells, anion substitutions

Semi-transparent solar cells are very attractive due to the increasing integration into our daily life. Kesterite-type based thin-film solar cells stand out because of its environmentally-benign composition and outstanding stability. Here, the influence of the back contact (Mo/V_2O_5/FTO or Mo/FTO) and thickness of $Cu_2ZnGe(S,Se)_4$ (CZGSSe) absorber layer, grown by sulfurization of co-evaporated CZGSe, is investigated. To increase the transparency, thinner absorber layers with higher band gap energy are produced. A double Sulfur-gradient through the CZGSSe layer with a considerable S content near the back contact and the formation of $Mo(S,Se)_2$ phase at the back interface is detected for an absorber of only 400 nm thickness. Efficiencies of 3.1 % and 2.7 % are achieved for 1.2 μm CZGSSe-based devices with E_g of 1.73 and 1.86 eV respectively, while enabling transmittance values higher than 20 % in the NIR. The highest transmittance, 40 % in the NIR, is achieved for the 400 nm CZGSSe-based solar cells with E_g of 2.1 eV; however, a significant reduction of these devices' performance is obtained due to the presence of ZnS secondary phase and a different back contact interface formation. This work presents the first promising semi-transparent CZGSSe solar cells, opening new paths of applications.

1. Introduction

One of the great challenges in our modern society is the supply of low-cost, environmentally friendly energy sources that can meet the growing demands of an expanding population. Photovoltaic (PV) is one of the main renewable energies to solve the energy crisis. The research on new materials and solar cell designs for different applications has received much attention in the last years. For example, semi-transparent solar cells can be used for Building Integrated Photovoltaic (BIPV), very attractive in residential, industrial and commercial buildings. In the last years, interest in agrovoltaics is also increasing. First semi-transparent solar cells are being used for agriculture applications, mainly using organic materials that can allow sunlight with selected wavelengths to pass through and get absorbed by the plants for the photosynthesis. [1] In addition, wide band gap (E_g) semi-transparent solar cells can be used as top cell of a multi-junction or tandem device, enhancing the efficiency of the PV devices.

Kesterite-type materials, $Cu_2ZnSn(S,Se)_4$ (CZTSSe), have gained interest to be used as absorber for thin-film solar cells in the last years because they consist of elements of low toxicity and high abundancy in the earth´s crust, having a high absorption coefficient and stability, and a tunable band gap energy E_g between 1.0 eV ($Cu_2ZnSnSe_4$) and 1.6 eV (Cu_2ZnSnS_4). Efforts to enhance the performance of CZTSSe are focused towards the reduction of the large open-circuit voltage (V_{OC}) deficit that are mainly caused by heterojunction interface recombination (kesterite/CdS); optimization of the bulk of the absorber band gap and potential fluctuations induced by Cu-Zn crystalline disorder; [2] and the presence of secondary phases, among other factors. [3-4] The introduction of Ag or Ge has led to the reduction of some specific defects. [3-5] As a result of these efforts recently, efficiencies higher than 14 % have been achieved for Ag-alloyed CZTSSe-based solar cells. [6]

As mentioned above, semi-transparent solar cells increase the range of applications, but it is a challenge to maintain a high efficiency and transparency at the same time. In the case of inorganic and stable semiconductors, the transparency can be increased by the use of a wide band gap material and/or by reducing the thickness of the active layer. With this objective in mind, it is very interesting to investigate wide band gap kesterite-type material on transparent substrates. Generally, the increase of E_g has been carried out by the substitution of Se by S and Sn by Ge, from E_g 1.45 eV [7] for CZGSe and around 2.2 eV for CZGS. [8] Se-rich devices with less than 40 % Ge exhibit the lowest V_{OC} and fill factor FF deficits with efficiencies beyond 13 %. [9] However, a little increase of Ge concentration leads to a significant decrease of solar cell efficiency. [4] Only few laboratories work in the fabrication of $Cu_2ZnGe(S,Se)_4$ (CZGSSe)-based thin-film solar cells, showing that the E_g value increases with the S concentration but leads to a significant reduction of the device performance and enhancement of the V_{OC} deficit. [10-14] S-rich wide band gap compounds are of great interest because of their contribution to the development of kesterite-based tandem solar cells and for the applications in BIPV and agrovoltaics already mentioned. However, it is necessary to optimize the sulfur concentration and its distribution through the absorber layer to improve the CZGSSe PV device performance [13-14]. The sulfurization of the surface of the absorber layer results in a higher E_g on the surface, increasing the V_{OC} and device efficiency. [13-15] Previously, we fabricated CZGSSe thin films by sulfurization of co-evaporated CZGSe layers onto Mo/SLG substrates, achieving CZGSSe-based solar cells of η = 3.2 % for E_g = 2 eV, [14] and it is the highest efficiency ever reported for kesterite semiconductor with such a high band gap value.

It is interesting to note that there are not so many works about kesterite solar cells on transparent electrodes. [16-24] Tin doped indium oxide, In_2O_3:SnO_2 (ITO) and fluorine doped tin oxide, SnO_2:F (FTO) are the most common TCOs used as transparent back contacts. Generally, higher efficiency is achieved when kesterite is grown on FTO as back electrode, because of the In diffusion into CZTSSe

layer and the formation of SnO_x when using ITO. [16] On the other hand, carrier loss in FTO is expected due to out diffusion of fluorine during annealing of the kesterite layer, forming a non-ideal back interface. [17] The addition of an interlayer, as Mo, MoO_3, between FTO and the active layer has demonstrated the enhancement of the device performance. For example, Espíndola-Rodríguez et al. [18] produced CZTSSe PV devices with performance of 6.3 % (front illumination) and of 7.7 % (bifacial illumination) grown on Mo (20 nm)/FTO with E_g of 1.09 eV. Becerril et al. [19] reported CZTSe, CZTS and CZTSSe solar cells deposited on FTO, obtaining efficiencies of 6.1%, 6.2%, and 7.9% (E_g = 1.47 eV in the latter), respectively. The use of transition metal oxides in those cases, such as TiO_2 and V_2O_5, together with a Mo:Na nanolayer improved the back interface. Later, Ruiz-Perona et al. [20] fabricated CZTGSe thin films by co-evaporation onto Mo/V_2O_5/FTO/glass followed by a thermal treatment in Se-atmosphere, achieving a device performance of 5.6 %, E_g = 1.28 eV and straight-through transmittance of 30 % in the near infrared (NIR) region. Following the same growth process, CZGSe thin films solar cells with efficiency of 5.3 %, E_g = 1.47 eV and total transmittance near 50 % in the NIR range were achieved. [21] Very recently, Zhou et al. [22] reported 11.4 % efficiency $(Ag,Cu)_2ZnSn(S,Se)_4$ (ACZTSSe) solar cells on MoO_3/FTO substrates, presenting the absorber layer a band gap energy of only 1.15 eV.

Therefore, the fabrication of high efficiency wide band gap kesterite solar cells is a challenge, being particularly difficult to maintain a high transparency. In this work, we integrate a wide band gap kesterite-type material (CZGSSe) with transparent back contacts to investigate the performance of semi-transparent $Cu_2ZnGe(S,Se)_4$ thin-film solar cells. Based on our previous experience, CZGSSe thin films are grown by sulfurization of co-evaporated CZGSSe on Mo/V_2O_5/FTO and Mo/FTO transparent back-contacts. Up to our knowledge, we have obtained the highest efficiencies ever reported for CZGSSe-based PV devices that are as high as 3.1 % and 2.7 % for bandgap values of E_g = 1.73 and 1.86 eV respectively on semi-transparent electrodes.

2. Results and Discussion

2.1. *CZGSSe thin films: back contact and absorber thickness effect*

Table 1 shows the composition and thickness of the prepared CZGSSe thin films with the different back-contact configurations, as measured by EDX. It is well-established that Cu-poor and Zn-rich are the optimal ranges of composition to produce high efficiency solar cells, [25] related to the formation of point defects and secondary phases. As shown in **Table 1**, the CZGSSe absorber layer deposited on Mo/V_2O_5/FTO/glass (sample 1) presents a Cu-poor and Zn-poor composition; however, the

samples 2 and 3 grown on Mo/FTO/glass are characterized by a more optimal composition to achieve high efficiency solar cells. Apart from the CZGSSe thickness, the main difference between samples 2 and 3 is the S concentration. Note, that despite that we have reduced the amount of S and GeS added during the sulfurization process due to the smaller thickness of the CZGSe layer of the sample 3 (2 mg S and 2 mg GeS for sample 3 versus 22 mg S and 6 mg GeS for samples 1 and 2), the S incorporation has been larger. It is 6 times larger for sample 3 than for sample 2. Therefore, it is found that upon reduction of the absorber thickness a proportionally smaller amount of S is needed during the sulfurization process to form the wide band gap CZGSSe material with the same composition.

Table 1. Description of the investigated samples (1-3): Composition of the CZGSSe absorber layer, deposited on different back contacts, measured by EDX at 25 kV operation voltage.

Sample nm	Back contact	Cu (at %)	Zn (at %)	Ge (at %)	Se (at %)	S (at %)	[Cu]/([Zn]+[Ge])	[Zn]/[Ge]	[S]/([S]+[Se])
1/1200	MVF	18.3	11.9	13.7	40.8	17.1	0.72	0.87	0.30
2/1200	MF	18.2	11.8	11.9	45.0	8.8	0.77	0.99	0.16
3/400	MF	18.8	12.2	11.8	17.2	40.0	0.78	1.04	0.70

Note: MVF (Mo/V_2O_5/FTO); MF (Mo/FTO)

The transparency is an essential parameter to consider for the fabrication of semi-transparent solar cells. There is a lack of information about transmittance measurements of semi-transparent kesterite thin films and kesterite-based PV devices in the literature. **Figure 1** shows the straight-through transmittance of CZGSSe/back contact structures together with those of FTO, V_2O_5/FTO, Mo/V_2O_5/FTO and Mo/FTO. The deposition of 15 nm of V_2O_5 on top of the commercial FTO reduces the straight-through transmittance in the whole wavelength range slightly, being more abrupt at wavelengths shorter than 500 nm. Finally, the deposition of around 15 nm of Mo on top of V_2O_5/FTO leads to a significant decrease of transmittance in the whole wavelength region. However, it is the

sputtered ~ 30 nm Mo directly on FTO that is the responsible of a more significant reduction of the transmittance compared to that induced by the vanadium oxide interlayer, as shown in **Figure 1**. The kesterite-type material deposited on the different back contacts investigated shows a transmittance higher than 20 % in the NIR. From **Figure 1** it is clear that a higher band gap energy E_g is obtained for sample 3. The lower band gap energy corresponds to sample 2, which agrees with the lower amount of S incorporated into the CZGSe lattice during the sulfurization process as measured by EDX and shown in **Table 1**. The transmittance increases somewhat when the S content increases. The higher transmittance is obtained for the thinner absorber layer in the NIR, which is also the CZGSSe film with higher S concentration. Therefore, the higher the E_g, the higher the transmittance in the whole wavelength range. But also, as shown above, it is necessary to take into account the semi-transparent back contact used. The higher transmittance of sample 1 is due to the higher S content, but also to the specific Mo/V_2O_5/FTO back-contact configuration used.

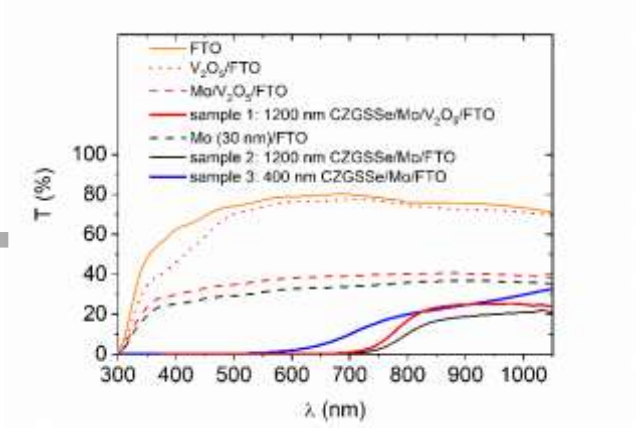

Figure 1. Straight-through transmittance of FTO, V_2O_5/FTO, Mo/V_2O_5/FTO, Mo/FTO and of the CZGSSe thin films grown on the different back-contact configurations.

Figure 2 shows GIXRD diffractograms of all the samples investigated by using grazing incidence angles of 1º and 4º. All of the diffraction patterns show Bragg peaks which can be attributed to the kesterite-type structure of CZGSSe, with different [S]/([S]+[Se]) atomic ratios, being the main diffraction peaks between those of CZGSe (01-070-7623) and CZGS (04-012-7580). Apart from the kesterite-type phase, $Ge(S,Se)_2$ as secondary phase was detected in all of the samples, especially in

samples 1 and 2 with the characteristic diffraction peaks at around 15º. Moreover, it is not possible to discard the presence of ZnS (01-071-5976) secondary phase for all the samples, especially for sample 3. The FTO substrate was also measured to identify the corresponding diffraction peaks in all the samples investigated. The presence of $MoSe_2$ at the back contact cannot be ruled out, independent of the back contact used. A zoom of the main 112 diffraction peak of CZGSSe is plotted for the three samples. The 112 Bragg peak is shifted towards higher diffraction angles when the measurements are performed at GI angle of 1º, indicating a higher S content at the surface region for all the samples. The 112 Bragg peak of samples 1 and 2 clearly show the presence of two CZGSSe phases with different [S]/([S]+[Se]) atomic ratios. The situation changes for the sample 3, only one phase of CZGSSe with much higher S content of around 70 % is present, in agreement with EDX measurements.

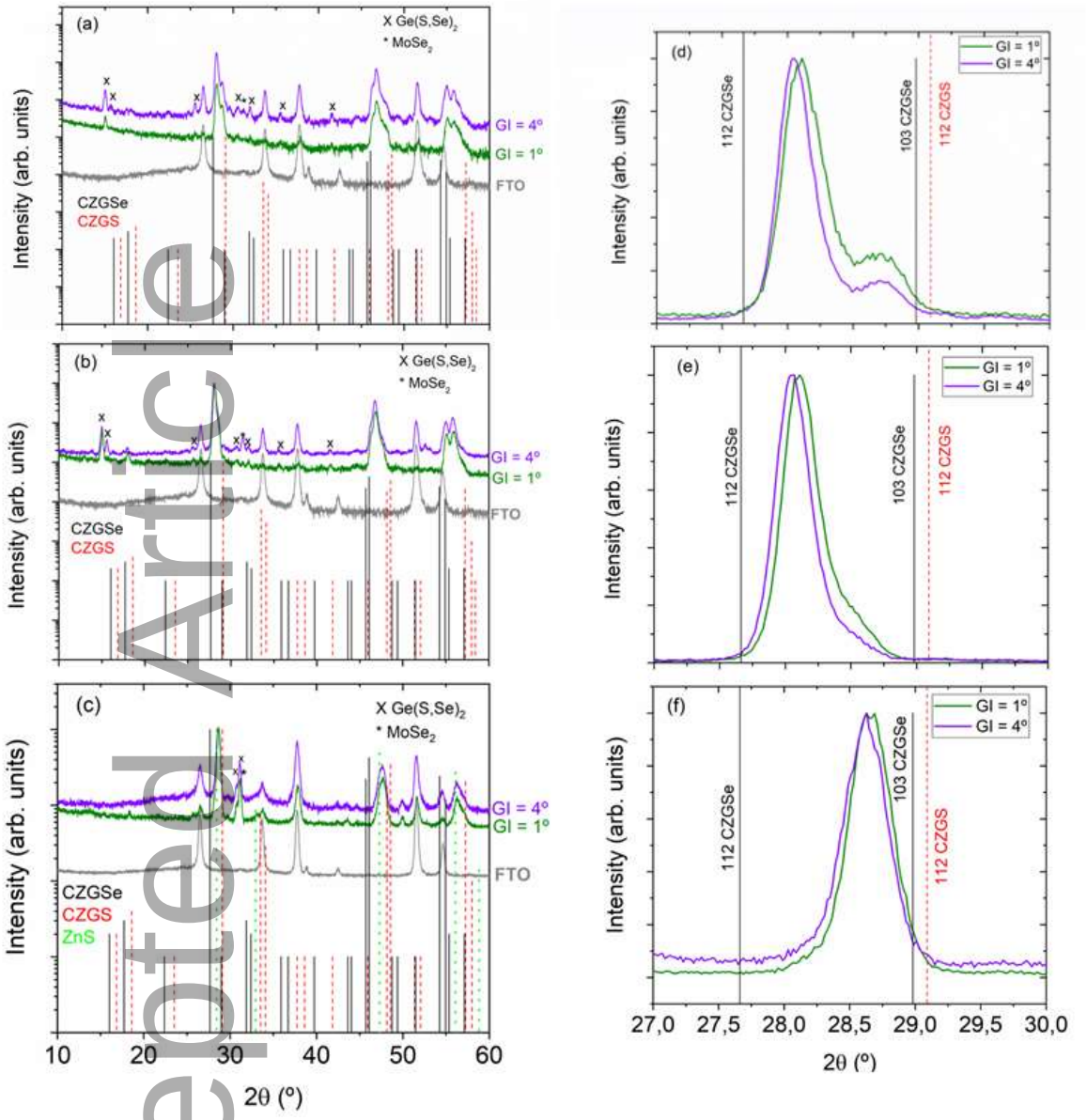

Figure 2. Grazing incidence X-ray diffractograms of CZGSSe grown on (a) Mo/V_2O_5/FTO (sample 1), (b) and (c) Mo/FTO (sample 2 and 3 respectively). Zoom of the 112 Bragg peak of CZGSSe corresponding to (d) sample 1, (e) sample 2 and (f) sample 3.

Figure 3 shows the in-depth elements distribution through the CZGSSe thin film for all the samples investigated. Measurements were carried out after optimizing the sputtering parameters according to the procedure described in. [26] A non-uniform distribution of the cations through the absorber layer 1 is observed (see **Figure 3.a.**). This distribution is very similar to that obtained previously for CZGSe thin films deposited on the same back contact (Mo/V_2O_5/FTO) configuration [21]. In the previous case,

the thermal treatment was performed under the same conditions as used in the present work but with the addition of elemental Se instead of S. In the near front region, a decrease of Cu and Zn and an increase of Ge GD-OES-signals take place. At the same location, an increase of the Na signal occurs, in agreement with the preference of Na for Cu vacancies, as reported previously. [21] A pronounced increase and decrease of S and Se signals respectively are detected from the bulk towards the surface. This may suggest the substitution of Se by S. Different from sample 1, in the case of sample 2, the in-depth distribution of the cations through the absorber thickness is more uniform, with a slight lower Cu signal near the surface. Similar to sample 1, an increase of the S and decrease of the Se GD-OES signals are detected towards the surface region. The cations distribution through the thickness of sample 3 is much more uniform, only detecting a slight increase of Zn and decrease of Cu GD-OES signals near the surface region. An interesting feature of sample 3 is the double S-gradient through the CZGSSe thickness with an increased S-signal measured near the back contact, different from the samples 1 and 2.

Figures 3.d-3.f. display the in-depth distribution of the normalized [S]/([S]+[Se]) atomic ratio for the three samples investigated. In all the cases, the ratio increases towards the surface region. The S content is higher for sample 1 than 2 as shown in Table 1, being this higher S concentration mainly accumulated at the surface. A steeper [S]/([S]+[Se])-gradient through the CZGSSe layer is measured for sample 1, which could indicate that the back contact plays a role on the S/Se distribution. It is well known the importance of the control of S/Se in-depth distribution to enhance V_{OC}. It has been reported that a higher S-content near the surface and a minimum S-content inside the space charge region results in a higher V_{OC} and efficiency η of CZTSSe-based solar cells. [27] From this point of view the absorber 1 shows a more favorable anions gradient for an increased efficiency.

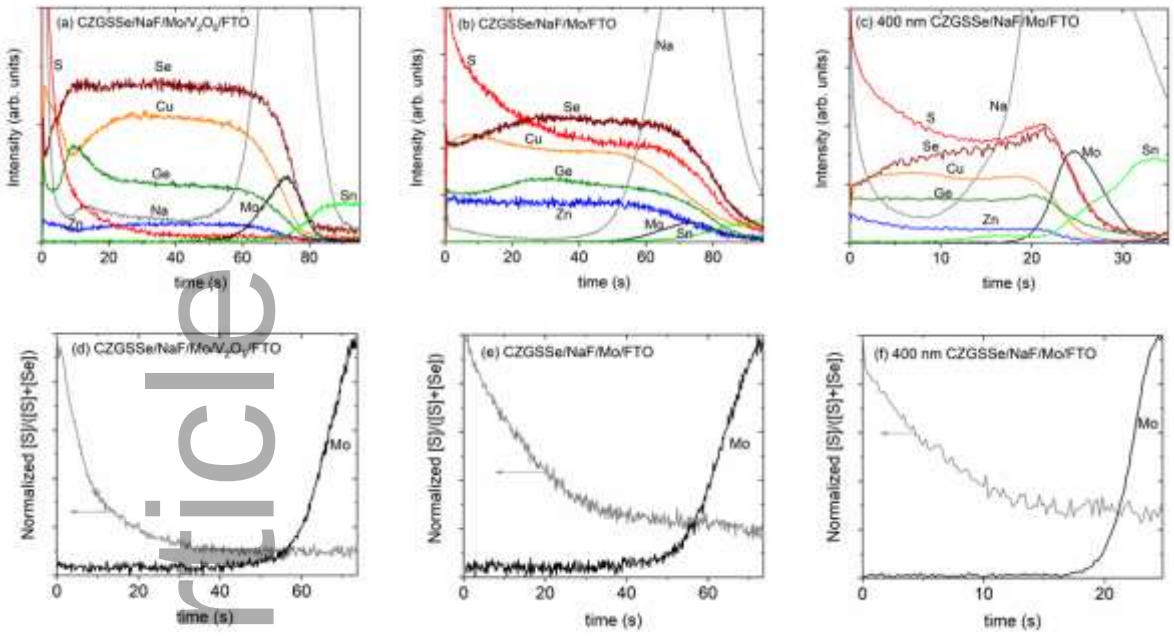

Figure 3. GD-OES depth profiles of Cu, Zn, Ge, Se, S of CZGSSe grown on (a) Mo/V_2O_5/FTO (sample 1), (b) and (c) Mo/FTO (samples 2 and 3 respectively). The normalized [S]/([S]+[Se]) atomic ratio versus sputtered time is plotted in (d), (e) and (f) for all the samples. The Mo in-depth profile has been also displayed to distinguish the back interface easily. The CZGSSe layer of (c) and (f) presents a thickness of 400 nm, while the thickness of the absorber film of (a), (b), (d) and (e) is of around 1200 nm.

Raman spectra of the three CZGSSe thin films are measured using 532 and 325 nm excitation wavelengths (see **Figure 4**). The measurements are carried out from the front and back side (through the glass substrate) of the samples. The spectra were measured in up to 15 points in each sample and the pale lines in the **Figure 4** represent the spectra from each point, while clear lines represent the average spectra.

Measurements under green excitation wavelength from the front side of the films show the presence of mainly CZGSSe phase at the surface of all samples (based on the presence of characteristic peaks of CZGSSe compound). [14, 28-29] Based on the shift of the main Raman peaks involving mainly Se-Se and S-Se vibrations and the change of the relative intensity of the peaks related to S-S vibrations

(the peaks ranges are indicated by arrows on top of **Figure 4**) the [S]/([S]+[Se]) atomic ratio is increasing from sample 2 to sample 1, and the sample 3 presents the highest one [28], in agreement with EDX and GIXRD measurements. In addition, some amount of $Ge(S,Se)_2$ secondary phase is present in all samples in good concordance with GIXRD measurements. [14] This means that effective composition of the kesterite phase will contain less Ge than measured by EDX, which shows the overall composition of the thin films.

The measurements performed from the back side of the films show the presence of the $MoSe_2$ phase (peaks at 169, 240 and 286 cm^{-1} [30]) in the samples 1 and 2 together with some pure CZGSe or a very Se-rich phase of CZGSSe solid solution (peaks at 183 and 209 cm^{-1}). [31] This indicates a gradient of the [S]/([S]+[Se]) ratio along the thickness of the samples 1 and 2, decreasing the S content towards the back side, as measured by GD-OES depth-profile. Also, the difference in the intensity of peaks corresponding to kesterite and $MoSe_2$ phases indicates the different thickness of the $MoSe_2$ layer in the two samples, thicker in sample 2 than in sample 1. This is related to the thicker Mo layer of around 30 nm of sample 2 than that used in sample 1. The sample 3 is very different from the other two samples, showing several peaks that can be assigned to a $Mo(S,Se)_2$ phase; peaks of CZGSSe can be also detected. This result agrees with the higher S content from the GD-OES signal measured next to the back contact for sample 3, explaining the formation of $Mo(S,Se)_2$ and of CZGSSe at the back interface. This indicates the sulfurization of the whole bulk of this thin film, but a gradient of [S]/([S]+[Se]) ratio cannot be excluded from these measurements, as it is confirmed by GD-OES depth-profiles. Therefore, the thinner CZGSSe thin film enhances the diffusion of the S through the thickness of the active layer in comparison to the obtained for samples 1 and 2, leading to a different back interface.

Finally, analysis of the spectra measured under UV excitation show clear presence of the ZnS phase at the surface of sample 3 [32] and the absence of this phase or of a Zn(S,Se) analogue phase at the surface of the other samples. [33]

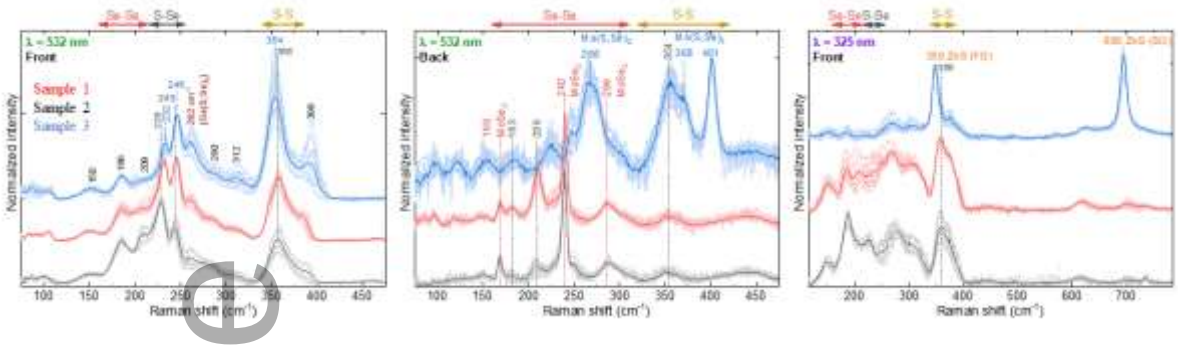

Figure 4. Raman spectra of CZGSSe thin films deposited on semi-transparent electrodes (sample 1: Mo/V_2O_5/FTO and samples 2 and 3: Mo/FTO) measured under 532 nm and 325 nm excitation wavelengths from the front and the back of the absorber/back contact structure. Peaks indicated with the numbers (peaks positions) belong to the CZGSSe phase; peaks of other phases always indicate the specific phase.

Cross-sectional SEM pictures of CZGSSe/Mo/V_2O_5/FTO/glass and CZGSSe/Mo/FTO/glass structures corresponding to the three samples investigated are shown in **Figure 5**. All of them present a compact and columnar structure without voids or adhesion problems at the back interface. Samples 1 and 2 are characterized by a larger grain size of the absorber layer, while sample 3, with a thickness of only 400 nm, also presents some brighter smaller grains. EDX measurements performed in the different grains reveal a higher Zn content in the brighter grains, in agreement with the presence of ZnS as detected by Raman spectroscopy measurements.

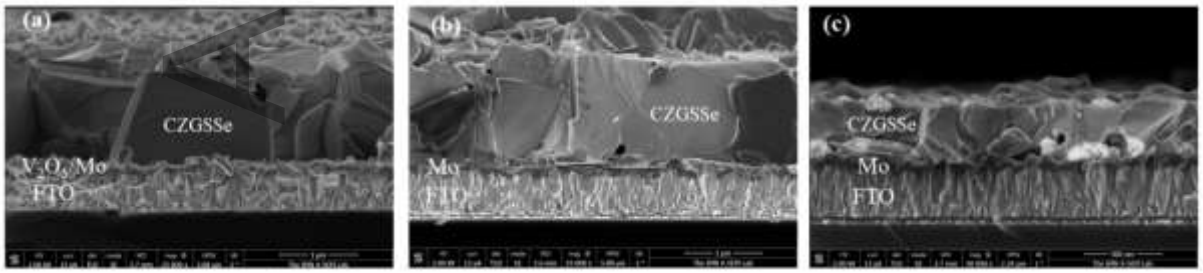

Figure 5. Cross-sectional SEM pictures of (a) CZGSSe (sample 1)/Mo/V_2O_5/FTO, (b) CZGSSe (sample 2)/Mo/FTO and (c) CZGSSe (sample 3)/Mo/FTO.

2.2. *CZGSSe -based solar cells: back contact and absorber thickness effect*

The current density-voltage (J-V) curves of the best performing CZGSSe-based solar cells by using the absorber layers grown on the different back-contact configurations are shown in **Figure 6.a.** **Table 2** summarizes the PV parameters of the best solar cells corresponding to **Figure 6.a.** A higher V_{OC} and FF was obtained for the device 1 deposited on Mo/V_2O_5/FTO/glass. However, the low short circuit current density J_{SC} reduces the maximum efficiency to a value of 2.7 %. The device 2 presents a higher J_{SC}, leading to an increased performance of 3.1 %. As mentioned above, with the objective of increasing the transparency of the solar cell, PV devices with only 400 nm of CZGSSe were fabricated (device 3). In that case, the maximum efficiency was of only 0.8 %, presenting worsen PV parameters.

Figure 6.b. shows external quantum efficiency EQE for the three devices of **Table 2**. The device 2 is characterized by the highest one in the whole range of wavelengths, in agreement with the reported J_{SC} values. The optical band gap energy (E_g) has been determined from the EQE measurements using the peak energy of the derivative of the EQE at longer wavelengths, and the values are shown in **Table 2**. The trend is that E_g increases with the S content (see **Table 1**). This is in good agreement with the results of Guo et al. [34] who reported that E_g increases linearly with the sulfur content in CZTSSe material. The higher J_{SC} for the device 2 than for device 1 can be related to the lower E_g for the sample 2. In any case, EQE curves start to decrease from around 500 nm on, indicating losses due to optical reflection and/or carrier collection, suggesting that the CdS/CZGSSe interface and the bulk of the CZGSSe material is not yet fully optimized. Sample 3 presents the higher E_g of 2.1 eV in agreement with the higher S concentration measured by EDX and determined by GIXRD and Raman spectroscopy; nevertheless, it is the device with the lowest V_{OC} and therefore, with the highest V_{OC}-deficit. Different reasons could explain the higher V_{OC}-deficit for the device 3, being difficult to identify which is the most critical factor. The sample 3 was characterized by the presence of ZnS secondary phase at the surface as measured by Raman spectroscopy, as well as by the formation of

smaller brighter Zn-rich grains as detected by SEM. Previously, it has been reported the influence of Zn(S,Se) secondary phase on the CZTSe, CZTS, CZTGSe-based devices performance. [35-37] While Shin et al. [35] reported that the presence of ZnS secondary phase at the back interface has a negligible effect on the electrical properties of the CZTS solar cells, devices with large grains of ZnS in the bulk of the absorber layer show a lower efficiency because of a reduced V_{OC}, J_{SC} and FF in. [36] More recently, the presence of ZnSe at the surface and in the bulk of CZTGSe photoactive layer resulted in a reduced V_{OC} and J_{SC}. [37] If ZnS would appear as an insulator phase, this would affect the J_{SC}, but it also affects to other PV parameters, then, its effect is due to other electronic effect to be investigated. But there are other factors that can be responsible for the lower V_{OC} and all the PV parameters.

The non-optimized double S-gradient through the CZGSSe layer, shown in **Figure 3.c.**, can be another reason for the lower V_{OC} for sample 3. The increase of the [S]/([S] + [Se]) atomic ratio is responsible for a higher E_g, but the optimization of the S-distribution through the active layer is one of the challenges to enhance V_{OC} and the solar cell efficiency. Another characteristic of this device 3 is the development of a different back interface with the formation of a $Mo(S,Se)_2$ layer because of the higher S content near the back contact. It is necessary to point out that the back interface is also very important to enhance the carrier collection, and here, it has been demonstrated that depends on the thickness of the absorber layer used. The use of a different back contact configuration and thickness of CZGSSe film could lead to a different alignment of $MoSe_2$ and $Mo(S,Se)_2$, that would affect specially to J_{SC} and FF of the solar cells. [38-39] It is the device 3 that presents much lower FF, that could be related with a different back interface reflected in the higher series resistance R_s value as shown in **Table 2**. The device 1 presents a higher FF, indicating the positive impact of adding an intermediate layer of V_2O_5 to enhance the Ohmic contact [19]. And not less important, the significant reduction of the thickness of the kesterite layer probably results in an enhanced back recombination, decreasing the J_{SC} and all the PV parameters of device 3, as displayed in **Table 2**.

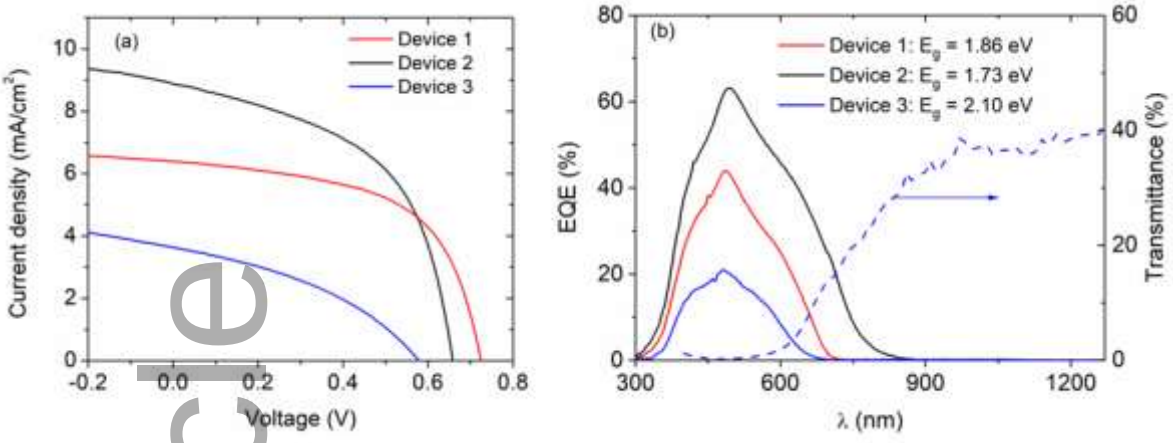

Figure 6. (a) Current density-voltage (J-V) curves and (b) external quantum efficiency measurements of the best three devices of the structures investigated. Transmittance of the completed device corresponding to device 3, FTO/Mo/CZGSSe (400 nm)/CdS/i-ZnO + ITO is also plotted.

Previously, we reported 1.3 µm CZGSSe thin films grown on Mo/SLG with an E_g of around 1.85 eV and an efficiency of 1.8 %, that is lower than that of devices 1 and 2, using the same absorber growth process as in the present work. [13] This result indicates that it is possible to fabricate semi-transparent wide band gap kesterite solar cells with higher efficiencies than using the Mo standard back contact and opens a wide range of applications. The straight-through transmittance of the completed device 3 is plotted in **Figure 6.b.**, reaching values near 40 % in the near-infrared region and with an average visible transmittance of ~ 7 %, being the highest transmittance obtained for CZGSSe-based PV devices, up to our knowledge. The transmittance of the completed device is higher than that of the bare absorber (see Figure 1). It indicates that the ITO and ZnO layers enhance the transmission of the optical structure due to light interference processes at the interfaces of the films forming the device, similar to what was observed for the $CuGaSe_2$-based solar cells.[40] An appropriate optical model should be developed in order to better explain this effect. Future work is geared towards the control of the sulfurization process to develop an optimized S-gradient through thin absorber layers that allows for increasing device performance at the same time as the transparency.

Table 2. PV parameters of the different CZGSSe photovoltaic devices investigated.

Device	Back contact	V_{OC} (mV)	J_{SC} (mA/cm^2)	FF (%)	η (%)	R_s ($\Omega \cdot cm^2$)	R_{sh} ($\Omega \cdot cm^2$)	E_g (eV)
1	MVF	724	6.4	57.7	2.7	4.3	997	1.86
2	MF	658	8.9	52.5	3.1	2.1	370	1.73
3	MF	576	3.6	38.5	0.8	6.5	403	2.10

Note: MVF (Mo/V_2O_5/FTO); MF (Mo/FTO)

3. Conclusion

CZGSSe thin films have been deposited by sulfurization of co-evaporated CZGSe layers on two different back contacts, Mo/V_2O_5/FTO and Mo/FTO, and their properties have been investigated in order to optimize the active layer properties and the corresponding solar cells performance. CZGSSe phase together with $Ge(S,Se)_2$ secondary phase have been identified by GIXRD and Raman spectroscopy measurements. All the CZGSSe thin films present a higher S content near the surface. The thinner CZGSSe grown on Mo/FTO presents a double S-gradient through the absorber layer thickness resulting in the formation of $Mo(S,Se)_2$ and in the presence of CZGSSe at the back interface, that are very different from previously investigated samples with micron-thickness layers. We report the fabrication of the first efficient semi-transparent CZGSSe-based solar cells. Efficiencies up to 3.1 %, 2.7 % and 0.8 % have been achieved for CZGSSe-based devices with E_g of 1.73, 1.86 and 2.10 eV respectively. The incorporation of V_2O_5 interlayer in the back contact structure leads to an enhanced FF of the PV device. The presence of ZnS secondary phase, the higher S content near the Mo/FTO back contact and the much thinner absorber layer of 400 nm are identified as the possible origin of the reduced efficiency of 0.8 %. Transmittance near 40 % in the near infrared region has been achieved for CZGSSe solar cells with 400 nm of absorber thickness and E_g of 2.10 eV. These results reveal the importance of the fine control of the sulfurization process for an improved device

performance. In future work it will be necessary an appropriate control of the proper S distribution and back interface, and to design strategies to avoid the formation of secondary phases that have a negative effect on the device performance.

4. Experimental Section

Back contact preparation: Commercial FTO-coated soda-line glass (Sigma Aldrich) with a sheet resistance of 7 Ω/sq and an optical transmission of 80 – 82 % in the visible range were used as the transparent back electrodes. Different back contact configurations were investigated. First, a Mo (15 nm)/V_2O_5 (15 nm)/FTO/glass structure was used, which allows for reducing the series resistance of the final solar cell. Previously, we have demonstrated that this back-contact configuration is very effective to obtain efficient CZGSe and CZTGSe-based solar cells. [20-21] Moreover, a more simplified back-contact structure was used, Mo with thicknesses of around 30 nm was deposited on top of FTO. The V_2O_5 layer was grown by thermal evaporation (Oerlikon Univex 250) with a deposition rate of 0.5 Å/s and a base pressure of 4 x 10^{-5} mbar. The Mo-layer was deposited by DC-magnetron sputtering (Alliance Concept CT100) using 4.2 W/cm² power density, at 1.3x10^{-3} mbar and at room temperature.

Absorber Synthesis: CZGSSe thin films were grown by sulfurization of co-evaporated CZGSe thin films. CZGSe thin films were co-evaporated from Cu, ZnSe, Ge and Se sources at a nominal substrate temperature of 150 ºC as described elsewhere. [21] The base pressure in the vacuum chamber was of 10^{-7} mbar, while the working pressure was in the range of 10^{-6} mbar. The thickness of the kesterite-type absorber layer was controlled by the evaporation time of CZGSe thin films. Samples of 1200 and 400 nm of thicknesses were selected for this work. A NaF precursor layer of around 12 nm was evaporated just before the co-evaporation of CZGSe thin films in the same vacuum chamber due to the beneficial effect of alkali elements on kesterite-based solar cells.

In order to obtain the CZGSSe thin films, the CZGSe layers were placed into a graphite box and sulfurized at 480 º C for 1 h under Ar atmosphere in a tubular furnace. 22 mg of S and 6 mg of GeS

were included in the graphite box in the case of the samples with thicknesses of around 1.2 µm (samples 1 and 2 in **Table 1**), [13-14] while only 2 mg of S and 2 mg of GeS were added in the case of the much thinner absorber layer of 400 nm (sample 3 in **Table 1**). GeS was added to avoid the loss of Ge at high temperature. The purpose of thinner kesterite layer was to increase the transparency of the solar cells.

Device fabrication: Before the CdS deposition, CZGSSe thin films were etched with KCN 2 % for 30 s. After that, a CdS buffer layer of around 50 nm of thickness was grown by chemical bath. A window layer composed of i-ZnO (50 nm) and In_2O_3:SnO_2 (ITO) (350 nm) layers was deposited by DC-pulsed sputtering deposition. Neither grids nor an anti-reflection coating were deposited onto the final photovoltaic devices. Moreover, no thermal treatment was performed to the solar cells.

Characterization: Energy dispersive X-ray spectroscopy (EDX) (Oxford instruments, model INCAx-sight) using a Hitachi S-3000N scanning electron microscope (SEM) was used to measure the chemical composition of the kesterite-type thin films. For that, operating voltages of 25 kV and the Cu K, Zn K, Ge K, Se K and S K lines were used for elemental quantification. The distribution of elements throughout the thickness of the kesterite absorber layer was measured via glow discharge optical emission spectrometry (GD-OES) using a Spectruma GDA 650. Depth profiles are collected using an Argon plasma in a pulsed RF mode for sputtering and a CCD-array for optical detection. The measurements were done without calibration samples, which is the reason for showing the depth profiles as qualitative plots. However, these enable a reliable comparison of the qualitative distribution of the containing elements in the kesterite layers, since all measurements were performed under the very same conditions. Grazing incidence X-ray diffraction (GIXRD) was performed to investigate the structural properties of the CZGSSe thin films and to identify the different phases. GIXRD data were collected with a PANAlytical X´Pert Pro MPD diffractometer, using CuK_α radiation and a multilayer mirror to produce a parallel beam. Detector scans with incident angles of

1º and 4º were carried out. The morphology of the CZGSSe/Mo/V_2O_5/FTO/glass structure was investigated by SEM using a SEM FEI VERIOS 460, operating at 2 kV. Raman scattering measurements of the CZGSSe solar cells were performed using FHR640 monochromator from Horiba Jobin-Yvon coupled with CCD camera. The measurements were performed in backscattering configuration through the probe designed at IREC using 325 and 532 nm lasers as excitation source. The laser power density did not exceed 80 W/cm^2. The spectral position was calibrated by imposing the main peak of monocrystalline Si to 520 cm^{-1}. Transmittance of the CZGSSe/back contact structures were measured with a Cary Varian 5000 spectrophotometer in the range from 300 to 1100 nm. The transmittance of the completed solar cell device was measured by using a spectroscopic ellipsometer (Woollam VASE) in the same wavelength range and using focussing probes that allows measurements in a selected circular area with a radius of 200 μm. Current-Voltage (*I-V*) characteristics of the photovoltaic devices were measured by using a Sun 3000 class solar simulator (Abet Technologies Inc., Milford, Connecticut, USA) under standard test conditions (25°C, AM 1.5, 100 mW/cm^2). External quantum efficiency (*EQE*) of the solar cells was measured using a Bentham PVE300 system (Bentham Instruments Ltd., Berkshire, UK) calibrated with a Si and Ge photodiodes.

Acknowledgements

CELL2WIN (PID2019-104372RB-C32), InnoPV (PID2022-140226OB-C33) funded by MCIN/AEI/ 10.13039/501100011033 and by "ERDF A way of making Europe". ASSESS (TED2021-129666B-C21 and C22) funded by MCIN/AEI/ 10.13039/501100011033 by the "European Union NextGenerationEU/PRTR". European Project INFINITE-CELL (H2020-MSCA-RISE-2017–777968). M.P. and M.G. acknowledge the financial support from the Spanish Ministry of Science, Innovation and Universities within the Ramón y Cajal (RYC-2017-23758) and Ramón y Cajal (RYC2022-035588-I) programs, respectively. ARP also acknowledges financial support from

Community of Madrid within Youth Employment Program (PEJD-2017-PRE/IND-4062). The authors would also like to thank Fátima Cabello and Marina García for technical support.

Received: ((will be filled in by the editorial staff))
Revised: ((will be filled in by the editorial staff))
Published online: ((will be filled in by the editorial staff))

References

[1] Y. Zhao, Y. Zhu, H.W. Cheng, R. Zheng, D. Meng, Y. Yang, *Materials Today Energy* **2021**, 22, 100852.

[2] R. Caballero, E. Garcia-Llamas, J.M. Merino, M. León, I. Babichuk, V. Dzhagan, V. Strelchuk, M. Valakh, *Acta Materialia* **2014**, 65, 412–417.

[3] S. Giraldo, Z. Jehl, M. Placidi, V. Izquierdo-Roca, A. Pérez-Rodríguez, E. Saucedo, *Adv. Mater.* **2019**, 31, 1806692.

[4] R. Scaffidi, G. Birant, G. Brammertz, J. de Wild, D. Flandred, B. Vermang, *J. Mater. Chem. A*, **2023**, 11, 13174–13194, and references inside.

[5] Y. E Romanyuk, S. G Haass, S. Giraldo, M. Placidi, D. Tiwari, D. J. Fermin, X. Hao, H. Xin, T. Schnabel, M. Kauk-Kuusik, P. Pistor, S. Lie, L. HWong, *J. Phys.: Energy* **2019**, 1 044004.

[6] J. Zhou, X. Xu, H. Wu, J. Wang, L. Lou, K. Yin, Y. Gong, J. Shi, Y. Luo, D. Li, H. Xin, Q. Meng, *Nat Energy* **2023**, 8, 526–535.

[7] S. Kim, K.M. Kim, H. Tampo, H. Shibata, K. Matsubara, S. Niki, *Sol. Energy Mater. Sol. Cells* 2016, 144, 488-492.

[8] E. Garcia-Llamas, J.M. Merino, R. Serna, X. Fontané, I.A. Victorov, A. Pérez-Rodríguez, M. León, I.V. Bodnar, V. Izquierdo-Roca, R. Caballero, *Sol. Energy Mater. Sol. Cells* **2016**, 158, 147-153.

[9] J. Wang, J. Zhou, X. Xu, F. Meng, C. Xiang, L. Lou, K. Yin, B. Duan, H. Wu, J. Shi, Y. Luo, D. Li, H. Xin and Q. Meng, Adv. Mater. **2022**, 34, 2202858.

[10] B. Vermang, G. Brammertz, M. Meuris, Th. Schnabel, E. Ahlswede, L. Choubrac, S. Harel, C. Cardinaud, L. Arzel, N. Barreau, J.van Deelen, P.J. Bolt, P. Bras, Y. Ren, E. Jaremalm, S. Khelifi, S. Yang, J. Lauwaert, M. Batuk, J. Hadermann, X. Kozina, E. Handick, C. Hartmann, D. Gerlach, A. Matsuda, S. Ueda, T. Chikyow, R. Félix, Y.Zhang, R. G. Wilks, M. Bär, *Sustainable Energy Fuels* **2019**, 3, 2246–2259.

[11] N. Saini, N. M. Martin, J.K. Larsen, A. Hultqvist, T. Törndahl, C. Platzer-Björkman, *Sol. RRL* **2022**, 6, 2100837.

[12] Th. Schnabel, M. Seboui, E. Ahlswede, *Energies* **2017**, 10, 1813.

[13] A. Ruiz-Perona, G. Gurieva, M. Sun, T. Kodalle, Y. Sánchez, M. Grossberg, J. M. Merino, S. Schorr, M. León and R. Caballero, *J. Alloys Compd*. **2021**, 868, 159253.

[14] A. Ruiz-Perona, M. Guc, Y. Sánchez, T. Kodalle, J. M. Merino, M. León and R. Caballero, *Sol. Energy* **2021**, 226, 251–259.

[15] C.H. Cai, S.W. Wei, W.C. Huang, C.H. Hsu, W.H. Ho, C.H. Lai, *Sol. Energy Mater. Sol. Cells* **2017**, 162, 21–29.

[16] J. Ge, J. Ghu, J. Jiang, Y. Yan, P. Yang, *ACS Sustain. Chem. Eng.* **2015**, 3, 3043–3052.

[17] S. W. Leow, W. Li, J. M. R. Tan, S. Venkataraj, V. Tunuguntla, M. Zhang, S. Magdassi, L. H. Wong, *Solar RRL*. **2021**, 5, 2100131.

[18] M. Espindola-Rodriguez, D. Sylla, Y. Sánchez, F. Oliva, S. Grini, M. Neuschitzer, L. Vines, V. Izquierdo-Roca, E. Saucedo, M. Placidi, *ACS Sustain. Chem. Eng.* **2017**, 5, 11516.

[19] I. Becerril-Romero, D. Sylla, M. Placidi, Y. Sánchez, J. Andrade-Arvizu, V. Izquierdo-Roca, M. Guc, A. Pérez-Rodríguez, S. Grini, L. Vines, B. Pusay, R. Almache, J. Puigdollers, P. Pistor, E. Saucedo, M. Espindola-Rodriguez, *ACS Appl. Mater. Interfaces* **2020**, 12 33656.

[20] A. Ruiz-Perona, Y. Sánchez, M. Guc, S. Khelifi, T. Kodalle, M. Placidi, J.M. Merino, M. León, R. Caballero, *Solar Energy* **2020**, 206, 555-563.

[21] A. Ruiz-Perona, Y. Sánchez, M. Guc, T. Kodalle, M. Placidi, J.M. Merino, F. Cabello, M.García-Pardo, M. León, R. Caballero, *J. Phys. Mater*. **2021**, 4, 034009.

[22] Y. Zhou, C. Xiang, Q. Dai, S. Xiang, R. Li, Y. Gong, Q. Zhu, W. Yan, W. Huang, H. Xin, *Adv. Energy Mater*. **2023**, 13, 2300253.

[23] S.N. Khan, S. Ge, E. Gu, S.K. Karunakaran, W. Yang, R. Hong, Y. Mai, X. Lin, G. Yang, *Adv. Mater. Interfaces* **2021**, 8, 2100971.

[24] S.N. Khan, S. Ge, Y. Huang, H. Xu, W. Yang, R. Hong, Y. Mai, E. Gu, X. Lin, G. Yan, *Sci China Mater* **2022**, 65 (3), 612-619.

[25] S. Schorr, G. Gurieva, M. Guc, M. Dimitrievska, A. Perez-Rodriguez, V. Izquierdo-Roca, C.S. Schnohr, J. Kim, W. Jo, J.M. Merino, *J. Phys Energy* **2020**, 2, 012002/40.

[26] T. Kodalle, D. Greiner, V. Brackmann, K. Prietzel, A. Scheu, T. Bertram, P. Reyes- Figueroa, T. Unold, D. Abou-Ras, R. Schaltmann, C.A. Kaufmann, V. Hoffmann, *J. Anal. Spectrom.* **2019**, 34, 1233–1241.

[27] K.J. Yang, D.H. Son, S.J. Sung, J.H. Sim, Y.I. Kim, S.N. Park, D.H. Jeon, J. Kim, D.K. Hwang, C.W. Jeon, D. Nam, H. Cheong, J.K. Kang, D.H. Kim, *J. Mater. Chem. A* **2016**, 4, 10151–10158.

[28] J.Andrade-Arvizu, R. Fonoll-Rubio, V. Izquierdo-Roca, I. Becerril-Romero, D. Sylla, P. Vidal-Fuentes, Z. J. Li-Kao, A. Thomere, S. Giraldo, K. Tiwari, S. Resalati, M. Guc, M. Placidi, *ACS Applied Materials and Interfaces* **2022**, 14, 1177-1186.

[29] D.Palma-Lafuente, P. Diez-Silva, V. Rotaru, T. Jawhari, T. Bertram, P. Reyes-Figueroa, M. Guc, J.M. Merino, R. Caballero, *Solar Energy Materials and Solar Cells* **2023**, 254, 112243.

[30] D. Nam, J.U. Lee, H. Cheong, *Scientific Reports* **2015**, 5, 17113.

[31] E. Grau-Luque, I. Anefnaf, N. Benhaddou, R. Fonoll-Rubio, I. Becerril-Romero, S. Aazou, E. Saucedo, Z. Sekkat, A. Perez-Rodriguez, V. Izquierdo-Roca, M. Guc, *Journal of Materials Chemistry A* **2021**, 9, 10466-10476.

[32] A. Fairbrother, V. Izquierdo-Roca, X. Fontané, M. Ibáñez, A. Cabot, E. Saucedo, A. Pérez-Rodríguez, *CrystEngComm* **2014**, 16, 4120-4125.

[33] M. Dimitrievska, H. Xie, A.J. Jackson, X. Fontané, M. Espíndola-Rodríguez, E. Saucedo, A. Pérez-Rodríguez, A. Walsh, V. Izquierdo-Roca, *Phys. Chem. Chem. Phys.*, **2016**, 18, 7632-7640.

[34] Q. Guo, G.M. Ford, W.C. Yang, C.J. Hages, H.W. Hillhouse, R. Agrawal, R., *Sol. Energy Mater. Sol. Cells* **2012**, 105, 132–136.

[35] B. Shin, O. Gunawan, Y. Zhu, N.A. Bojarczuk, S.J. Chey, S. Guha, *Prog. Photovolt. Res. Appl.* **2013**, 21, 72–76.

[36] J. Just, D. Lützenkirchen-Hecht, R. Frahm, S. Schorr, T. Unold, *Appl. Phys. Lett.* **2011**, 99, 262105.

[37] A. Ruiz-Perona, Y. Sánchez, M. Guc, L. Calvo-Barrio, T. Jawharic, J.M. Merino, M. León, R. Caballero, *Sol. Energy* **2020**, 199, 864-871.

[38] R. Würz, D. Fuertes-Marrón, A. Meeder, A. Rumberg, S.M. Babu, Th. Schedel-Niedrig, U. Bloeck, P. Shubert-Bischoff, M.Ch. Lux-Steiner, *Thin Solid Films* **2003**, 431-432, 398-402.

[39] R. Caballero, C.A. Kaufmann, T. Eisenbarth, A. Grimm, I. Lauermann, T. Unold, R. Klenk, H.W. Shock, *Appl. Phys. Lett.* **2010**, 96 092104.

[40] R. Caballero, S. Siebentritt, K. Sakurai, C.A. Kaufmann, M. Ch. Lux-Steiner, 2006 IEEE 4th World Conference on Photovoltaic Energy Conversion **2006**,1, 479-482.

Table of content

Efficient semi-transparent CZGSSe thin-film solar cells with performance of 3.1 and 2.7 % and E_g = 1.73 and 1.86 eV are fabricated. The reduction of the absorber thickness to 400 nm results in a higher transparency of ~ 40 % in the NIR, but also in lower devices efficiency because of the different back-interface and ZnS phase formation.

*Andrea Ruiz-Perona[1, +], David Palma-Lafuente[1], Yudania Sánchez[2], Maxim Guc[2], Tim Kodalle[3, x], Mohamed Ould Salem[2], Marcel Placidi[2,4], Rosalia Serna[5], Alejandro Pérez-Rodríguez[2,6], José Manuel Merino[1], Raquel Caballero[1,5]**

WILEY-VCH

Semi-transparent wide band gap $Cu_2ZnGe(S,Se)_4$ thin-film solar cells: Role of the sulfurization process